

Article

β -Cyclodextrin-Encapsulated Rhodamine Derivatives Core–Shell Microspheres—Based Fluorescent Sensor for Au³⁺ and Template for Generating Microplates of Gold

Maniyazagan Munisamy^{1,2,†}, Balamurugan Rathinam^{3,†}, Esakkimuthu Shanmugasundaram¹, Vigneshkumar Ganesan¹, Vimalasruthi Narayanan¹, Suganya Bharathi Balakrishnan¹, Selvam Kaliyamoorthy^{4,*} and Stalin Thambusamy^{1,*}

- ¹ Department of Industrial Chemistry, School of Chemical Sciences, Alagappa University, Karaikudi 630003, India; manichemist@gmail.com (M.M.); asmuthu92@gmail.com (E.S.); gvkumar.chemist@gmail.com (V.G.); annamsruthi2014@gmail.com (V.N.); sbsuganyaa@gmail.com (S.B.B.)
- ² Department of Nanotechnology and Advanced Materials Engineering, Sejong University, Seoul 05006, Republic of Korea
- ³ Department of Chemical and Materials Engineering, National Yunlin University of Science and Technology, Yunlin 64002, Taiwan; balar@yuntech.edu.tw
- ⁴ Department of Chemistry for Materials, Graduate School of Engineering, Mie University, Tsu 514-8507, Japan
- * Correspondence: chemsel@gmail.com (S.K.); stalin.t@alagappauniversity.ac.in (S.T.)
- † These authors contributed equally to this work.

Abstract: We have developed β -cyclodextrin-encapsulated rhodamine derivative core-shell microspheres (β -CD@RH) to improve their aqueous solubility and biocompatibility. The β -CD@RH core-shell microspheres exhibited bright and stable fluorescence with Au³⁺ ion in aqueous media. The development of triangular and hexagonal gold microplates within an aqueous solution by a simple, one-step, and green chemistry strategy is followed and prepared. Fluorescent imaging of Au³⁺ in living cells is also successfully demonstrated.

Keywords: fluorescent core-shell microspheres; β -cyclodextrin; rhodamine derivative; Au³⁺ detection; bioimaging



Citation: Munisamy, M.; Rathinam, B.; Shanmugasundaram, E.; Ganesan, V.; Narayanan, V.; Balakrishnan, S.B.; Kaliyamoorthy, S.; Thambusamy, S. β -Cyclodextrin-Encapsulated Rhodamine Derivatives Core–Shell Microspheres—Based Fluorescent Sensor for Au³⁺ and Template for Generating Microplates of Gold. *Micromachines* **2023**, *14*, 1443. <https://doi.org/10.3390/mi14071443>

Academic Editor: Wing-Cheung (Roy) Law

Received: 7 June 2023
Revised: 12 July 2023
Accepted: 14 July 2023
Published: 18 July 2023



Copyright: © 2023 by the authors. Licensee MDPI, Basel, Switzerland. This article is an open access article distributed under the terms and conditions of the Creative Commons Attribution (CC BY) license (<https://creativecommons.org/licenses/by/4.0/>).

1. Introduction

Gold (Au) has been one of the precious metals to humans since ancient times because of its esthetic qualities. Au³⁺ ions have been found to have a lot of interesting therapeutic properties and have been utilized to treat rheumatoid and TB arthritis in very small amounts [1]. However, the Au cations, Au³⁺ especially, are reported to be toxic toward human and aquatic species at high concentrations [2,3]. The toxicity of soluble Au³⁺ is due to its propensity to bind selectively to enzymes and DNA [4,5]. Au³⁺ is accountable for enzyme protein and depletion denaturation against selective cellular targets and lysosomal dysfunction, which results in the damage of DNA and membrane subsequently [6]. Au³⁺ also enhances oxidative DNA damage by catalyzing the production of free radicals in a variety of chemical entities employed in biochemical and biological studies [7]. To comprehend the real-world application of the sensors, the detection of Au³⁺ ions in complex and physiologically and ecologically significant solvents, in this case, phosphate buffer solution, was performed [8]. Therefore, the development of sensing tools that may be used for the selective detection of Au³⁺ over other interfering metal ions with very high sensitivity is highly desirable. In this regard, the literature contains a greater number of reviews on the detection of Au³⁺ in both aqueous and organic media [9,10]. Sensing Au³⁺ ion in an aqueous media is beneficial to identify the contamination in biological systems.

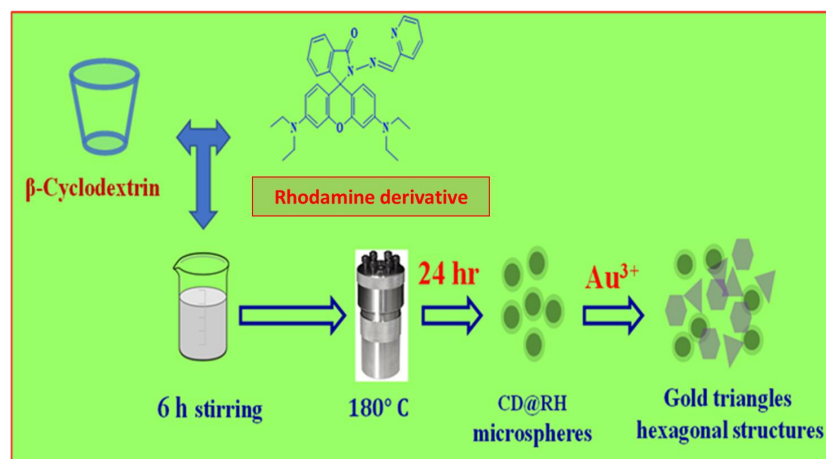
Among the various fluorescent probes designed for the recognition of Au³⁺, the fluorescence mode is advantageous due to its operational ultra-sensitivity and simplicity [11].

Moreover, the disaggregation-based fluorescence probe for Au (III) was simple to construct and showed excellent sensitivity, selectivity, and quick response time. Au (III) in cells can also be found using a probe or a paper-based strip [12]. Additionally, the latter complex binds to serum albumin and causes the typical CD bands to show in the visible spectrum. It has been shown that coordination at the level of the surface histidines is responsible for adduct formation for both of these gold (III) complexes [13]. The in-depth investigation of gold drug metabolism in vivo is studied the quick conversion of Au^{3+} to Au^+ by thiol proteins in organisms. Here, they are addressed by an in vitro and in vivo luminescent Au^{3+} probe (RA) based on the ruthenium (II) complex [14].

Cyclodextrins are cyclic oligosaccharides that have a hydrophilic surface area and a hydrophobic central cavity, favoring the formation of inclusion complexes with low-polarity organic molecules [15]. However, compared to the cyclodextrin family, β -cyclodextrin is known for its give better applications in the pharmaceutical field, owing to a simple drug complexation at low costs. The formation of cyclodextrin inclusion complexes with either water-insoluble or poorly soluble drug/organic molecules can increase overall water solubility and stability, enhance bioavailability and decrease the toxicity of related substances [16]. Moreover, recently most researchers have reported that microplates are used in different applications such as tissue engineering, biosensor, bioimaging, and pharmaceutical industries due to the controllable structures can enhance the hydrophilic and hydrophobic nature, high surface-to-volume ratio, and biocompatibility.

Many classes of molecular fluorescence chemo sensors have already been reported for metal ions detection [17,18]. Spiro lactam rhodamine-based chemo sensors have recently gained a lot of attention due to their great fluorescence characteristics, such as long absorption and emission wavelengths as a dye, good absorption coefficient, and high fluorescence quantum yield [19]. Research on the advancement of fluorescent probes for the selective detection of Au^{3+} has been gaining a lot of interest. Nevertheless, various flaws in these fluorescent sensing systems, such as cross-sensitivity to other metal cations, low water solubility, sluggish response, low fluorescence cytotoxicity, and enhancement, obstruct their optional functioning. There is a need to create new fluorescent probes for gold ions that may overcome these limitations.

In the present work, we have synthesized β -Cyclodextrin-Rhodamine derivative (β -CD@RH) based core-shell microspheres through a hydrothermal process (Scheme 1). The β -CD@RH core-shell microspheres exhibited good stability in an aqueous phase. Moreover, the β -CD@RH core-shell microspheres showed high sensitivity and selectivity towards Au^{3+} in an aqueous medium as verified by fluorescence studies and therefore the present probe may serve as a fluorescent sensor for recognition of Au^{3+} in living cells. To identify the β -CD@RH core-shell microspheres, we redirected the microsphere as an interior template to cultivate Au triangle and hexagonal microplates.



Scheme 1. Scheme of the synthetic procedure for generating β -CD@RH microspheres.

2. Materials and Methods

Rhodamine derivative (RH) was synthesized based on the reported procedure [20]. Rhodamine derivative (RH) was obtained by refluxing 2-pyridinecarboxaldehyde with rhodamine B hydrazide, in 77% yield (Scheme S1, ESI[†]). Synthesized fluorescent probe RH was further confirmed by standard spectroscopic techniques such as ¹H and ¹³C NMR spectroscopy, as well as ESI-MS (Figures S1–S3, ESI[†]). Further, the framework of RH was as certified by X-ray diffraction analysis. RH crystallized in the P21/c space group, which is monoclinic (CCDC no: 1440773) (Figure S4, Table S1, ESI[†]). An aqueous solution of β-CD (1 mmol) and an ethanol solution of RH (1 mmol) was mixed for 6 h at room temperature in a traditional experiment for the synthesis of β-CD@RH core-shell microspheres. After that, the β-CD@RH solution was transferred to a Teflon-lined stainless-steel autoclave (100 mL) and heated to 180 °C for 24 h. Scanning electron microscopy (SEM) and transmitting electron microscopy (TEM) were used to examine the generated β-CD@RH core-shell microspheres.

2.1. General Information and Materials

All of the materials for synthesis were purchased from commercial suppliers and used without further purification. The absorption spectra were recorded on a Shimadzu UV-PC-2401 UV-vis spectrophotometer using 10 mm path length quartz cuvettes in the range 300–800 nm wavelengths, while the fluorescence measurements were carried on a Horiba Jobin-Yvon FluoroMax-4 spectrofluorometer using 10 mm path length quartz cuvettes with a slit width of 5 nm at 298 K. FT-IR spectra were measured on a JASCO FTIR 4600 FT-IR spectrometer with 4 cm⁻¹ resolution and 32 scanned between wave number 4000 cm⁻¹ and 400 cm⁻¹. Samples were prepared KBr disks with 1 mg of complex in 100 mg of KBr. The mass spectra of RH using Agilent Technologies 6520 Accurate mass spectrometer. NMR spectra were recorded on a Varian FT-400 MHz instrument. The chemical shifts were recorded in parts per million (ppm) on the scale. The following abbreviations are used to describe spin multiplicities in ¹H NMR spectra: s = singlet; d = doublet; t = triplet; m = multiplet.

2.2. Synthesis of the Sensor Molecule (RH)

Rhodamine-B hydrazide (0.46 g, 1 mmol) was dissolved in 20 mL absolute ethanol. An excessive 2-Pyridinecarboxaldehyde (4 mmol) was added, and then the mixture was refluxed in an air bath for 6 h. After that, the solution was cooled (concentrated to 10 mL) and allowed to stand at room temperature overnight. The precipitate which appeared next day was filtered and washed 3 times with 10 mL of absolute ethanol. After drying under reduced pressure, the reaction afforded 0.47 g of RH (77%) as pink solid, mp (°C): 218 ± 2. ¹H NMR [CDCl₃, SiMe₄, J (Hz), δ (ppm)]: ¹H NMR (300 MHz, CDCl₃) δ 8.46 (d, J = 5.8 Hz, 1H), 8.00 (d, J = 8.1 Hz, 2H), 7.60 (t, J = 7.7 Hz, 1H), 7.52–7.40 (m, 2H), 7.12 (t, J = 6.5 Hz, 2H), 6.55 (d, J = 8.8 Hz, 2H), 6.45 (d, J = 2.4 Hz, 2H), 6.24 (dd, J = 8.8, 2.5 Hz, 2H), 3.31 (q, J = 7.1 Hz, 8H), 1.14 (t, J = 7.1 Hz, 12H). ¹³C NMR (75 MHz, CDCl₃) δ 165.61 (s), 153.43 (s), 152.60 (s), 145.97 (s), 136.30 (s), 128.46 (s), 108.58 (s), 105.85 (s), 98.54 (s), 77.66 (s), 77.23 (s), 44.52 (s), 12.61 (s). ESI mass: calculated value for [(C₃₄H₃₅N₅O₂) H] (M + H) is 545.67, experimental value 546.3 (Figures S1–S3, ESI[†]). The displacement ellipsoids created at the 30% probability level clearly show the X-ray crystal structure of RH evident. And with the crystal packing of RH, the hydrogen atoms have been eliminated for clarity. For clarity, intermolecular interactions have an outing of that (Figure S4, ESI[†]).

2.3. Synthesis of β-CD@RH Microspheres

The β-CD@RH core-shell microspheres were prepared according to the following procedure. Typically, 1 mmol of β-Cyclodextrin was dissolved in deionized water (solution A). One mmol of RH dye was dissolved in 10 mL acetonitrile. The obtained solution was added into solution A drop by drop and stirred for 6 h under ambient conditions. The prepared clear solution was then transferred into a 100 mL Teflon-lined stainless-steel

autoclave and maintained at 180 °C for 24 h. After cooling to room temperature, a brown suspension was obtained, which was centrifuged at 8000 rpm for 10 min and washed three times with DI water and ethanol. Finally, the precipitate was collected and dried in an oven at 80 °C overnight, which is noted as β -CD@RH microspheres.

2.4. Cell Culture

The Mesenchymal stem cells (C3H10T1/2) were purchased from National Centre for Cell Sciences (NCCS), Pune, India. The cells were plated at 7×10^5 per 25 cm² flask, maintained in Dulbecco's modified Eagle's medium (DMEM) supplemented with 10% fetal bovine serum (FBS) and 1% Penicillin/Streptomycin (10,000 U/mL) and maintained in a humidified incubator at 37 °C and 5% CO₂.

2.5. In Vitro Cytotoxicity

The cytotoxicity of the β -CD@RH microspheres, Au³⁺ and β -CD@RH-Au³⁺ were studied using MTT (3-(4,5-dimethylthiazol-2-yl)-2,5-diphenyltetrazolium bromide) assay on Mesenchymal stem cells. In brief, 10,000 cells/well in 100 μ L final volume was seeded into 96 well plates, once the cells were 70% confluent the media was removed and washed with PBS (Phosphate buffer saline) and replaced with serum-free media. The sterilized films ($n = 5$) were placed gently into each well above the cells and wells without the β -CD@RH microspheres were regarded as control. After 24 h of incubation, the wells were emptied and 10 μ L of MTT reagent from stock (5 mg/mL in PBS) was added to each well reaching a final concentration of 0.5 mg/mL. Then the cells were incubated for 2 h at 37 °C in a 5% CO₂ Incubator. After incubation the wells were emptied again and 200 μ L DMSO was added to each well to dissolve the insoluble purple formazan crystals. The 96 well plate was placed on a rocker for 20 min and then measured spectrophotometrically in an ELISA reader at a wavelength of 570 nm.

3. Results and Discussion

The SEM images of the β -CD@RH core-shell microspheres are shown in Figure 1a,b. The average diameter of the CD@RH core-shell microspheres is 650 to 900 nm. An SEM picture of β -CD@RH microspheres shown in Figure 1b, 2 μ m diameter is the enlarger image. It is evident that the microsphere SEM image. The β -CD@RH core-shell microspheres were dispersed perfectly in an aqueous solution; no aggregation was noticed due to the electrostatic repulsion power between the β -CD@RH core-shell microspheres. TEM was used to evaluate the morphology and size of the β -CD@RH core-shell microspheres and the TEM pictures are shown in Figure 1. As shown in Figure 1c, the TEM picture of β -CD@RH core-shell microspheres shows that the β -CD@RH microspheres are spherical with great distribution, and the average size of the β -CD@RH is 0.46 to 0.52 μ m. Then, measured the particle size distribution of the material, which is observable at 346 nm, and measured the mean physical size of the particles. DLS measurements showed that the average of the β -CD@RH core-shell microspheres was 750 nm, and this particle size value is a bit bigger than our particle size distribution result. The histogram highlighted in yellow in Figure 1d is part of the manuscript and have included in Figure S5, ESI†. The Zeta potential evaluation can be an imperative factor for checking the balance of β -CD@RH core-shell microspheres within the aqueous medium. The findings of the zeta potential experiments for β -CD@RH core-shell microspheres are shown in Figure S6 (ESI†). As is seen in Figure S6 (ESI†), the zeta potential value for β -CD@RH core-shell microspheres were found to be -42.2 mV. The β -CD@RH core-shell microspheres possess a sizable negative zeta potential value, as the particles are likely to repel one another and have improved suspension stability thereby. It is obvious that the probe β -CD@RH core-shell microspheres were colorless in an aqueous solution, had no apparent absorption, and was non-fluorescent, indicating that the spirocyclic form of the dye was dominant. The colorless and non-fluorescent solution progressively became pink in color and began to fluorescent under UV light with the addition of Au³⁺ (50 mM, 1 equivalent, regarding probe β -CD@RH). With the addition of

Au^{3+} , a new absorption band located at 556 nm (Figure 2a) and a strong fluorescence band at 582 nm (Figure 2c) related to the delocalized xanthene moiety of rhodamines appeared. It is important not to rule out the feasible involvement of additional metal ions in the sensing process. Therefore, the titration of the probe $\beta\text{-CD@RH}$ with various other metal ions was completed under the same sensing conditions. To our delight, related metal ions such as Ni^{2+} , Hg^{2+} , Co^{2+} , Fe^{2+} , Ca^{2+} , Cd^{2+} , Mg^{2+} , Cu^{2+} , Al^{3+} , and Fe^{3+} did not trigger any ring-opening reaction to lead to a spectroscopic response. Only in the presence of Au^{3+} did the fluorescence and absorption spectra alter significantly. Moreover, no significant color or spectral changes in $\beta\text{-CD@RH}$ solution were noticed with the addition of other metal ions demonstrating the high selectivity of the probe towards Au^{3+} ion. The RH is a dye that contains nitrogen; typically, nitrogen has a lone pair of electrons, making it most likely to impart a negative charge to the microspheres. Since metal ions have potential, the negative of RH is that ready attracted by a positive metal ion charge.

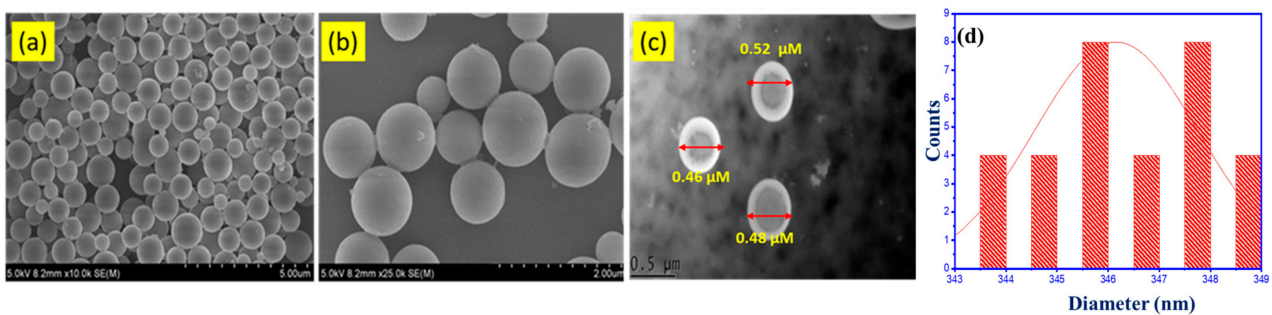


Figure 1. SEM image of $\beta\text{-CD@RH}$ microspheres (a,b). TEM images of $\beta\text{-CD@RH}$ microspheres (c) Average size distribution of $\beta\text{-CD@RH}$ microspheres(d).

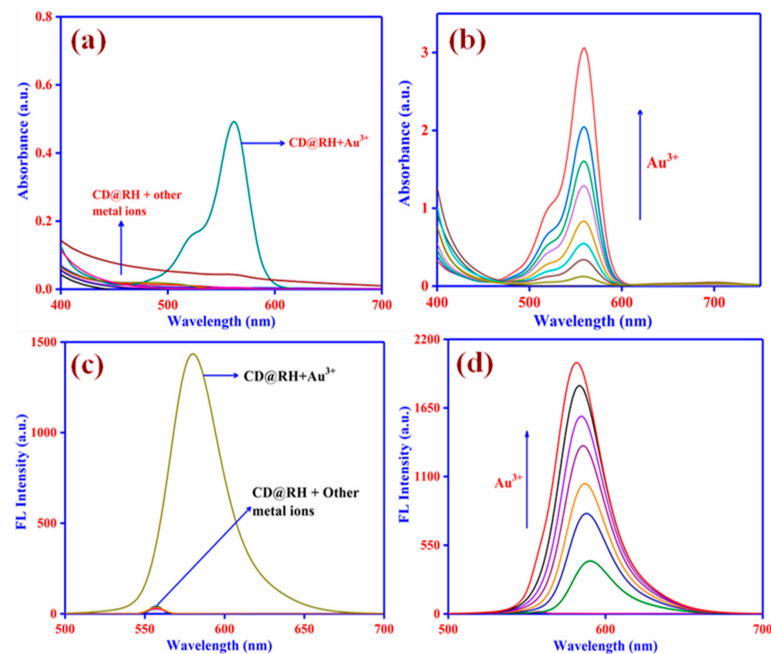


Figure 2. (a) UV–vis absorption spectra of $\beta\text{-CD@RH}$ microspheres observed upon addition of different metal ions (Ni^{2+} , Hg^{2+} , Co^{2+} , Fe^{2+} , Ca^{2+} , Cd^{2+} , Mg^{2+} , Cu^{2+} , Al^{3+} , Fe^{3+} and Au^{3+}) in aqueous solution. (b) UV–vis titration spectra of $\beta\text{-CD@RH}$ microspheres upon addition of Au^{3+} in aqueous solution (0 to 2 equiv.). (c) Changes of the fluorescence emission of $\beta\text{-CD@RH}$ microspheres observed upon addition of different metal ions (Ni^{2+} , Hg^{2+} , Co^{2+} , Fe^{2+} , Ca^{2+} , Cd^{2+} , Mg^{2+} , Cu^{2+} , Al^{3+} , Fe^{3+} and Au^{3+}) in aqueous solution. (d) Fluorescence titration spectra of $\beta\text{-CD@RH}$ microspheres upon addition of 0 to 2 equiv. of Au^{3+} in aqueous solution ($\lambda_{\text{ex}} = 556 \text{ nm}$).

The titration of Au^{3+} against probe $\beta\text{-CD@RH}$ core-shell microspheres gave a strong absorbance and fluorescence improvement with the addition of the Au^{3+} ions (Figure 2b). In the concentration range of 1–100 mM, the fluorescence titration profile of the probe $\beta\text{-CD@RH}$ core-shell microspheres with Au^{3+} showed a strong linear relationship, showing that the probe $\beta\text{-CD@RH}$ is suitable for quantitative evaluation. The detection limit was determined to be 0.6 parts per million. The enhancement of emission intensity was not observed above 100 mM of Au^{3+} . Although the spectroscopic response of the $\beta\text{-CD@RH}$ core-shell microspheres was quite sluggish, the entire saturation of the fluorescence intensity strength was observed after 60 min. The $\beta\text{-CD@RH}$ solution showed intense fluorescence with an approximately 10-fold enhancement in the fluorescence intensity at 590 nm. That is the fact the $\beta\text{-CD@RH}$ could use as an off-on fluorescent chemosensor for Au^{3+} .

A pH investigation was carried out to regulate the performance of the fluorescent probe $\beta\text{-CD@RH}$ by optimizing the pH of the experimental condition. In the absence of Au^{3+} ions, the fluorescent probe, $\beta\text{-CD@RH}$ exhibited fragile fluorescence and showed pH independency over the pH range 4.0–10.0 (Figure S7, ESI⁺). At low pH, the probe demonstrated high emission intensity because at low pH the spirolactam band opens irrespective of metal ions added. Nevertheless, it is noticed that the presence of Au^{3+} . However, it has here shown the emission intensity of $\beta\text{-CD@RH}$ at pH 4.0–10.0 is selectively increased by the presence of Au^{3+} ions. By keeping the $\beta\text{-CD@RH}$ core-shell microspheres and Au^{3+} ions constant (10 mM) and altering the mole fraction of Au^{3+} ions from 0 to 1, the Job's plot method for the absorbance was used to calculate the binding stoichiometry of the $\beta\text{-CD@RH-Au}^{3+}$ complex (Figure S8, ESI⁺). The absorbance maxima moved through a maximum at a molar fraction of nearly 0.5, suggesting that a 1:1 stoichiometry is most likely for the binding mechanism of $\beta\text{-CD@RH}$ core-shell microspheres and Au^{3+} , according to the Job's plot. The above results illustrate that the probe $\beta\text{-CD@RH}$ core-shell microspheres exhibited an excellent binding capability towards the Au^{3+} ions. The optical properties of the materials using the absorption and emission range of $\beta\text{-CD@RH}$ and $\beta\text{-CD@RH-Au}^{3+}$. The molar extinction coefficient (ϵ_{max}) and fluorescence quantum yield (Φ_{F}) are displayed in Table S1. The $\beta\text{-CD@RH-Au}^{3+}$ has a high ϵ_{max} value compared to the $\beta\text{-CD@RH}$, and the $\beta\text{-CD@RH}$ complex has a higher fluorescence behavior following the addition of Au^{3+} , as indicated by the Φ_{F} value.

In order to ascertain the selectivity of the probe toward Au^{3+} , several competitions experiments were performed where the probe $\beta\text{-CD@RH}$ core-shell microspheres were utilized for the sensing of Au^{3+} in the presence of other competing metal ions (Figure S9, ESI⁺). The results indicated that these ions showed no apparent interference in the Au^{3+} detection. Thus, the $\beta\text{-CD@RH}$ core-shell microspheres exhibited excellent selectivity toward Au^{3+} , which is essential for biological sensing applications. The entire sensing process is suggested to be reaction based and irreversible. To confirm this argument, a surplus quantity of S^{2-} ion (Na_2S (100 mM)) was put through the colored and fluorescent solution containing Au^{3+} and probe $\beta\text{-CD@RH}$. There were no noticeable changes either in the absorbance or fluorescence intensity after the addition of the sulfide ion, which indicates that the sensing process is irreversible (Figure S10, ESI⁺). In particular, when a rhodamine derivative adjoined with other organic moieties gives rise to a rhodamine derivative that may be enduring in two isomeric forms; one of the isomers exists as spirolactam with open ring structure (extended large π -conjugation arrangement) another one being ring closed (limited π -conjugation arrangement). However, the optical properties of both isomers are entirely different in that the ring's closed form is non-fluorescent and colorless. Furthermore, the association of metal ions transforms the specific spirolactam ring open which gives intense color and fluorescence through extended π -conjugation between the rhodamine derivative and metal anion. This notable characteristic furnishes an ideal model for conserving the OFF-ON mechanism. Here, β -cyclodextrin used as a carrier or core-shell of rhodamine derivatives, have a peculiar physicochemical property in its hydrophobic interior and hydrophilic exterior. Those properties and behaviors capable

of sensing the Au⁺ ions may be due to the presence of outermost electronic configurations. The limit of detection (LOD) was determined in response to your suggestion using the following formula:

$$\text{LOD} = 3.3 (\text{Sy}/\text{S}) \quad (1)$$

Sy is the response's standard deviation, and S is the slope of the linear curve. As a result, when the relationship between Au (III) concentration level and absorbance intensity, the graph plotted and obtained the linearity, and this curve to finding the LOD, this is shown in Figure S11. The β -CD@RH core-shell microspheres detection of Au (III) the LOD value is 38 nm. Recently, Atul Kapoor's research team members have proposed the AIEE active Azomethine-based rhodamine derivative for fluorimetrically and electrochemically LOD is 40 nm [21]. Here we also report the β -CD has introduced detection limit decreased, and the solubility is enhanced.

When the β -CD@RH-Au³⁺ solution is slowly aged, an appreciable quantity of precipitate was produced at the bottom of the vial. As the focus exceeds the templating character of the β -CD@RH core-shell microspheres alter their work as an exterior template to create Au microplates. The assumption is that the nucleation of Au ions was initiated on the top of β -CD@RH core-shell microspheres when it was completely saturated with Au ions. Once Au nuclei were created on its surface, they grow by consuming the Au³⁺ ions around them continuously and giving the Au microplates. As shown in Figure 3a–d, SEM photographs of the sample revealed that the gold microplates are mostly triangular and hexagonal shapes. The average size of the microplates is 0.9–1.3 μm . The microplates retain their shape and are stable for several days. The β -CD@RH core-shell microspheres play an important role in the creation of Au microplates, according to this research.

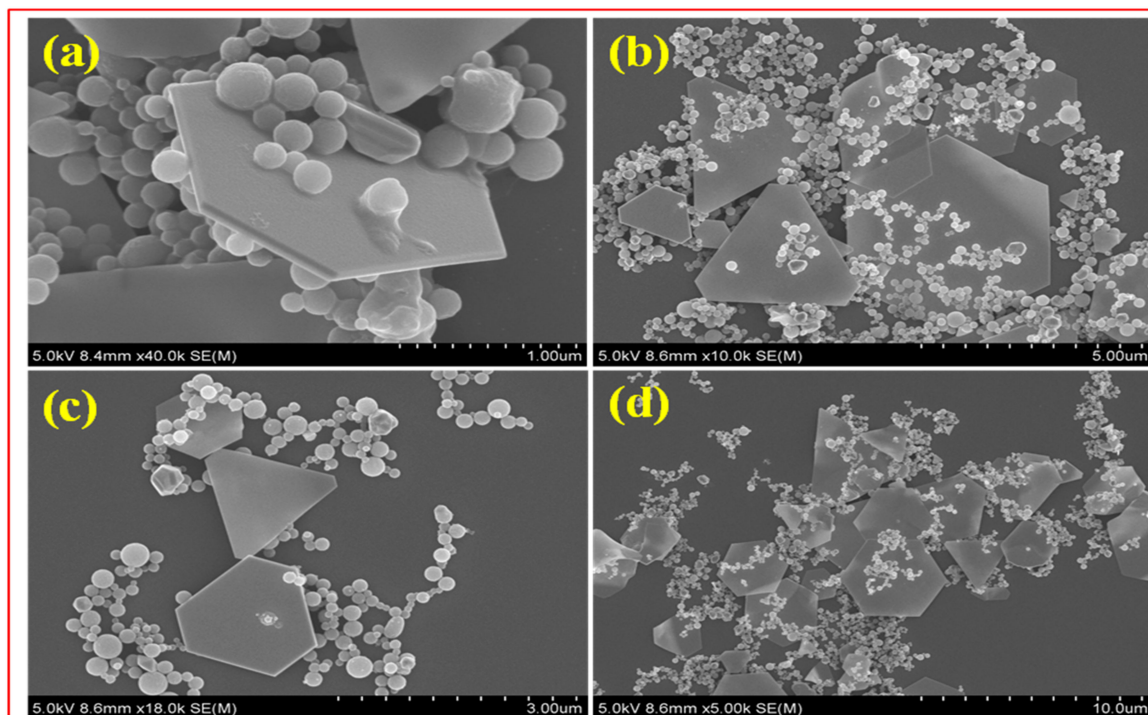


Figure 3. Scanning Electron Microscopy images of gold microplates. The sample's images in (a–d) showed that nearly all of the gold microplates are triangular and hexagonal, with an average microplate size of 0.9–1.3 μm . For several days, the microplates are stable and retain their shape.

Encouraged by all these attractive properties as evidenced by spectroscopic data that the probe can selectively sense Au³⁺ in an aqueous medium with a quick response, and also, evaluated the features of the probe β -CD@RH core-shell microspheres for imaging Au³⁺ in living cells. The typical MTT assay showed that the probe β -CD@RH microspheres at

the micromolar concentrations exhibited no cytotoxicity to the cells, and therefore it could be utilized as a probe for cell imaging. Mesenchymal Stem Cells (MSCs) (C3H10T1/2) were treated with probe β -CD@RH core-shell microspheres for 30 min before adding Au^{3+} and incubating for another 30 min. The fluorescence pictures were taken before and following the addition of Au^{3+} (10 mM) (Figure 4). MSCs incubated with probe β -CD@RH core-shell microspheres and Au^{3+} showed no fluorescence, whereas cells stained with probe β -CD@RH- Au^{3+} showed a strong fluorescence signal, indicating that the probe β -CD@RH core-shell microspheres is cell membrane permeable and can be efficiently used for in vitro imaging of Au^{3+} ions in living cells. Furthermore, there were no such indications of cell harm by β -CD@RH core-shell microspheres. The cells were intact and showed healthful adherent and also passed on morphology after and during the labeling procedure with probe β -CD@RH, indicating a lack of cytotoxic effects (Figure S12, ESI†). To better understand various metabolic processes and increase disease detection, it is essential to quantify the concentration and track the distribution of metal ions in individual cells, organs, and entire organisms. Among the various techniques for metal ion detection, fluorescent sensors using β -cyclodextrin-encapsulated rhodamine derivatives have drawn a lot of interest because of their many advantages, including operating simplicity, high sensitivity, quick detection speed, and real-time detection. This research highlights recent advancements in metal ions in biological systems, especially Au^{3+} .

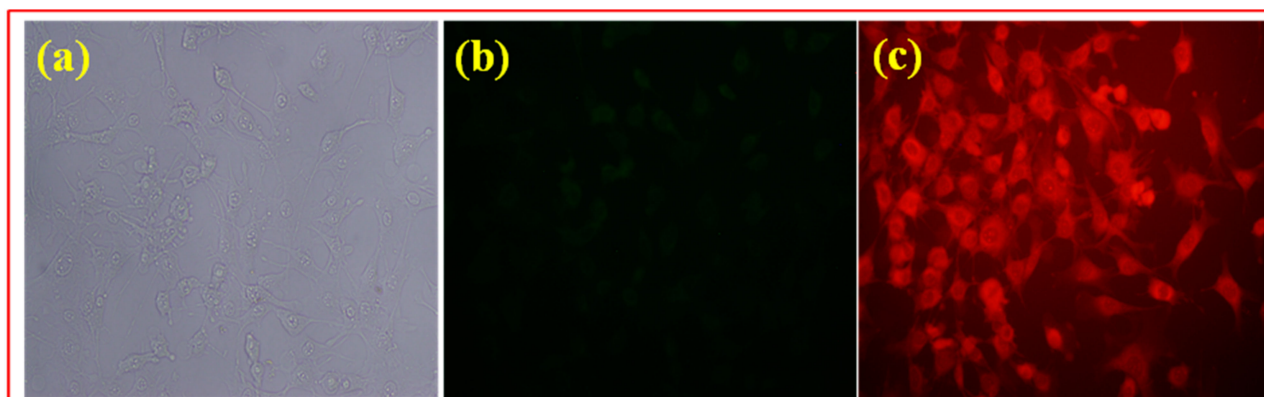


Figure 4. Fluorescence microscopic images of Mesenchymal stem cells (MSCs); (a) MSCs incubated with a probe β -CD@RH microspheres; (b) MSCs incubated with Au^{3+} ions; and (c) MSCs incubated with a probe β -CD@RH microspheres in the presence of Au^{3+} ions.

4. Conclusions

In conclusion, we have developed a β -CD@RH core-shell microsphere based on rhodamine derivative and β -cyclodextrin describing its extremely selective and sensitive fluorescence sensing nature towards Au^{3+} ions in an aqueous medium for the first time. The fluorescent probe β -CD@RH core-shell microspheres can be used to sense selectively Au^{3+} ions over other biologically relevant metal ions. The β -CD@RH core-shell microspheres could serve as a template to create a triangle and hexagonal gold microplates. The successful demonstration of Au^{3+} fluorescence imaging in living cells has been performed in this study. We anticipate the β -CD@RH core-shell microspheres could make a fluorescence probe for tracking Au^{3+} ions. Last but not least, the NMR analyses validate the development of the fluorescent probe RH. The packing of RH's crystals is also better understood because of the X-ray crystal structure and analysis. These studies have been by Dynamic Laser Scattering, Zeta Potential, competition experiments between Au^{3+} and specific metal ions, and the Cytotoxic effect.

Supplementary Materials: The following supporting information can be downloaded at: <https://www.mdpi.com/article/10.3390/mi14071443/s1>, 1. Experimental section, Scheme S1. Synthetic scheme for fluorescent probe RH., Figure S1. ¹H NMR (CDCl₃) of RH, Figure S2. ¹³C NMR of RH(CDCl₃), Figure S3. The ESI mass spectra of RH, Figure S4. (a) X-ray crystal structure of RH showing displacement ellipsoids drawn at the 30% probability level. Hydrogen atoms have been omitted for clarity. (b) The crystal packing of RH. Intermolecular interactions have been omitted for clarity, Figure S5. Dynamic laser scattering of β-CD@RH microspheres, Figure S6. Zeta potential of β-CD@RH microspheres, Figure S7. Fluorescence response of β-CD@RH in the absence and in the presence of Au³⁺ ions in water media at different pH (λ_{em} = 582 nm), Figure S8. Job's plot from the absorption data for stoichiometry determination between β CD@RH and Au³⁺ ions in water at 25 °C at λ_{abs} = 556 nm, Figure S9. Results of the competition experiments between Au³⁺ and selected metal ions. The free β-CD@RH concentration was set at 10 μM, and the excitation was at 556 nm with a slit width of 5.0 nm. Figure S10. UV–vis titration spectra of β-CD@RH (10 μM) with 5 equiv. of Au³⁺ upon the addition of sodium sulfide (30 μM) in water. Figure S11. (a) Concentration variation of Absorbance intensity Vs. Concentration of Al³⁺ (0 to 2 equiv.). (b) Concentration variation of FL intensity Vs. Concentration of Al³⁺ (0 to 2 equiv.), Figure S12. Cytotoxic effect of β-CD@RH, Au³⁺ and β-CD@RH-Au³⁺ in Mesenchymal Stem Cells (MSCs) incubated for 6 h by MTT assay. Results are expressed as the mean of three independent experiments, Table S1. Crystal data and details of refinements for RH.

Author Contributions: M.M.—Conceptualization, Methodology, Investigation, Writing—Original draft. B.R.—Investigation, E.S.—Investigation and analysis. V.G.—Revision and corrections. V.N.—Correction; draft carried out. S.B.B.—Formal analysis, Resources, S.K.—Supervision, S.T.—Supervision, Writing—review & editing. All authors have read and agreed to the published version of the manuscript.

Funding: Maniyazagan Munisamy is grateful to the DST-SERB (Science and Engineering Research Board) India, under the scheme of National Postdoctoral Fellowship Scheme [Project No: PDF/2017/002644] carry out this work. The Ministry of Science, ICT, and Future Planning financed this research through grants from the National Research Foundation of Korea (NRF) [NRF-2018K1A4A3A01064272] and [NRF-2020R1A6A1A03038540].

Data Availability Statement: The data presented in this study are available on request from the corresponding author.

Conflicts of Interest: The authors declare no conflict of interest.

References

1. Lee, H.; Lee, M.-Y.; Bhang, S.H.; Kim, B.-S.; Kim, Y.S.; Ju, J.H.; Kim, K.S.; Hahn, S.K. Hyaluronate–Gold Nanoparticle/Tocilizumab Complex for the Treatment of Rheumatoid Arthritis. *ACS Nano* **2014**, *8*, 4790–4798. [[CrossRef](#)]
2. Goodman, C.M.; McCusker, C.D.; Yilmaz, T.; Rotello, V.M. Toxicity of Gold Nanoparticles Functionalized with Cationic and Anionic Side Chains. *Bioconjugate Chem.* **2004**, *15*, 897–900. [[CrossRef](#)] [[PubMed](#)]
3. Nam, S.-H.; Lee, W.-M.; Shin, Y.-J.; Yoon, S.-J.; Kim, S.W.; Kwak, J.I.; An, Y.-J. Derivation of guideline values for gold (III) ion toxicity limits to protect aquatic ecosystems. *Water Res.* **2014**, *48*, 126–136. [[CrossRef](#)] [[PubMed](#)]
4. Marcon, G.; Carotti, S.; Coronello, M.; Messori, L.; Mini, E.; Orioli, P.; Mazzei, T.; Cinellu, M.A.; Minghetti, G. Gold (III) complexes with bipyridyl ligands: Solution chemistry, cytotoxicity, and DNA binding properties. *J. Med. Chem.* **2002**, *45*, 1672–1677. [[CrossRef](#)] [[PubMed](#)]
5. Bailes, J.; Gazi, S.; Ivanova, R.; Soloviev, M. Protein Immobilization on Gold Nanoparticles: Quantitative Analysis Methods. *Mol. Biol.* **2012**, *2118*, 199–211.
6. Sabella, S.; Carney, R.P.; Brunetti, V.; Malvindi, M.A.; Al-Juffali, N.; Vecchio, G.; Janes, S.M.; Bakr, O.M.; Cingolani, R.; Stellacci, F.; et al. A general mechanism for intracellular toxicity of metal-containing nanoparticles. *Nanoscale* **2014**, *6*, 7052–7061. [[CrossRef](#)] [[PubMed](#)]
7. Habib, A.; Tabata, M.J. A turn-on fluorescent probe for Au³⁺ based on rodamine derivative and its bioimaging application. *Inorg. Biochem.* **2004**, *57*, 1043–1047.
8. Kumeria, T.; Santos, A.; Losic, D. Ultrasensitive Nanoporous Interferometric Sensor for Label-Free Detection of Gold(III) Ions. *ACS Appl. Mater. Interfaces* **2013**, *5*, 11783–11790. [[CrossRef](#)]
9. Yuan, L.; Lin, W.; Yang, Y.; Song, J. A fast-responsive fluorescent probe for detection of gold ions in water and synthetic products. *Chem. Commun.* **2011**, *47*, 4703–4705. [[CrossRef](#)]
10. Dong, M.; Wang, Y.-W.; Peng, Y. Highly Selective Ratiometric Fluorescent Sensing for Hg²⁺ and Au³⁺, Respectively, in Aqueous Media. *Org. Lett.* **2010**, *12*, 5310–5313. [[CrossRef](#)]

11. Saha, K.; Agasti, S.S.; Kim, C.; Li, X.; Rotello, V.M. Gold Nanoparticles in Chemical and Biological Sensing. *Chem. Rev.* **2012**, *112*, 2739–2779. [[CrossRef](#)]
12. Kim, N.H.; Won, M.; Kim, J.S.; Huha, Y.; Kim, D. A highly sensitive and fast responsive fluorescent probe for detection of Gold(III) ions based on the AIEgen disaggregation. *Dyes Pigment.* **2019**, *160*, 647–653. [[CrossRef](#)]
13. Marcon, G.; Messori, L.; Orioli, P.; Cinellu, M.A.; Minghetti, G. Reactions of gold(III) complexes with serum albumin. *Eur. J. Biol. Inorg. Chem.* **2003**, *270*, 4655–4661. [[CrossRef](#)] [[PubMed](#)]
14. Xie, Z.; Wen, J.; Sun, S.; Zhang, J.; Deng, X.; Han, S.; Wang, L.; Zhang, B.; Hong, C.; Sun, S. In-vitro and in-vivo monitoring of gold(III) ions from intermediate metabolite of sodium aurothiomalate through water-soluble ruthenium (II) complex-based luminescent probe. *Bioorganic Chem.* **2021**, *110*, 104749. [[CrossRef](#)]
15. Loftsson, T.; Duchêne, D. Cyclodextrins and their pharmaceutical applications. *Int. J. Pharm.* **2007**, *329*, 1–11. [[CrossRef](#)]
16. Priya, A.S.; Sivakamavalli, J.; Vaseeharan, B.; Stalin, T. Improvement on dissolution rate of inclusion complex of Rifabutin drug with β -cyclodextrin. *Int. J. Biol. Macromol.* **2013**, *62*, 472–480. [[CrossRef](#)]
17. Du, J.; Hu, M.; Fan, J.; Peng, X. Fluorescent chemodosimeters using “mild” chemical events for the detection of small anions and cations in biological and environmental media. *Chem. Soc. Rev.* **2012**, *41*, 4511–4535. [[CrossRef](#)] [[PubMed](#)]
18. Shellaiah, M.; Chen, Y.-T.; Thirumalaivasan, N.; Azaad, B.; Awasthi, K.; Sun, K.W.; Wu, S.-P.; Lin, M.-C.; Ohta, N. Pyrene-Based AIEE Active Nanoprobe for Zn^{2+} and Tyrosine Detection Demonstrated by DFT, Bioimaging, and Organic Thin-Film Transistor. *ACS Appl. Mater. Interfaces* **2021**, *13*, 28610–28626. [[CrossRef](#)]
19. Na Kim, H.; Lee, M.H.; Kim, H.J.; Kim, J.S.; Yoon, J. A new trend in rhodamine-based chemosensors: Application of spirolactam ring-opening to sensing ions. *Chem. Soc. Rev.* **2008**, *37*, 1465–1472. [[CrossRef](#)]
20. Maniyazagan, M.; Mariadasse, R.; Jeyakanthan, J.; Lokanath, N.K.; Naveen, S.; Premkumar, K.; Muthuraja, P.; Manisankar, P.; Stalin, T. Rhodamine based “turn-on” molecular switch FRET-sensor for cadmium and sulfide ions and live cell imaging study. *Sens. Actuators B Chem.* **2017**, *238*, 565–577. [[CrossRef](#)]
21. Kapoor, A.; Pratibha; Rajpute, J.K.; Kumar, A. AIEE Active Azomethine-Based Rhodamine Derivative for Ultrasensitive Multichannel Detection of Au^{3+} Through a Fluorimetrically, Electrochemically, and RGB-Based Sensing Assay. *Anal. Chem.* **2023**, *95*, 5796–5806. [[CrossRef](#)] [[PubMed](#)]

Disclaimer/Publisher’s Note: The statements, opinions and data contained in all publications are solely those of the individual author(s) and contributor(s) and not of MDPI and/or the editor(s). MDPI and/or the editor(s) disclaim responsibility for any injury to people or property resulting from any ideas, methods, instructions or products referred to in the content.